

# Background Matters Too: A Language-Enhanced Adversarial Framework for Person Re-Identification

Kaicong Huang<sup>1</sup>, Talha Azfar<sup>1</sup>, Jack M. Reilly<sup>1</sup>, Thomas Guggisberg<sup>2</sup>, Ruimin Ke<sup>1</sup>

<sup>1</sup>Rensselaer Polytechnic Institute

<sup>2</sup>Capital District Transportation Authority

## Abstract

Person re-identification faces two core challenges: precisely locating the foreground target while suppressing background noise and extracting fine-grained features from the target region. Numerous visual-only approaches address these issues by partitioning an image and applying attention modules, yet they rely on costly manual annotations and struggle with complex occlusions. Recent multimodal methods, motivated by CLIP, introduce semantic cues to guide visual understanding. However, they focus solely on foreground information, but overlook the potential value of background cues. Inspired by human perception, we argue that background semantics are as important as the foreground semantics in ReID, as humans tend to eliminate background distractions while focusing on target appearance. Therefore, this paper proposes an end-to-end framework that jointly models foreground and background information within a dual-branch cross-modal feature extraction pipeline. To help the network distinguish between the two domains, we propose an intra-semantic alignment and inter-semantic adversarial learning strategy. Specifically, we align visual and textual features that share the same semantics across domains, while simultaneously penalizing similarity between foreground and background features to enhance the network’s discriminative power. This strategy drives the model to actively suppress noisy background regions and enhance attention toward identity-relevant foreground cues. Comprehensive experiments on two holistic and two occluded ReID benchmarks demonstrate the effectiveness and generality of the proposed method, with results that match or surpass those of current state-of-the-art approaches.

## Introduction

Person Re-identification (ReID) aims to match the same person across different scenes and camera views. Due to environmental complexity, the main challenges arise from diverse viewpoints, pose variations, background interference, and occlusions (Ning et al. 2024). Addressing these challenges boils down to a single objective: learning fine-grained feature representations that are both robust to noise and invariant to diverse perturbations. More precisely, (1) how to locate the target’s foreground while ignoring background disturbances; and (2) how to extract fine-grained features from that foreground region. Extensive efforts have been made to achieve this objective, which can be grouped into two major directions: model-driven and data-driven approaches (Tan et al. 2024). Model-driven methods focus on

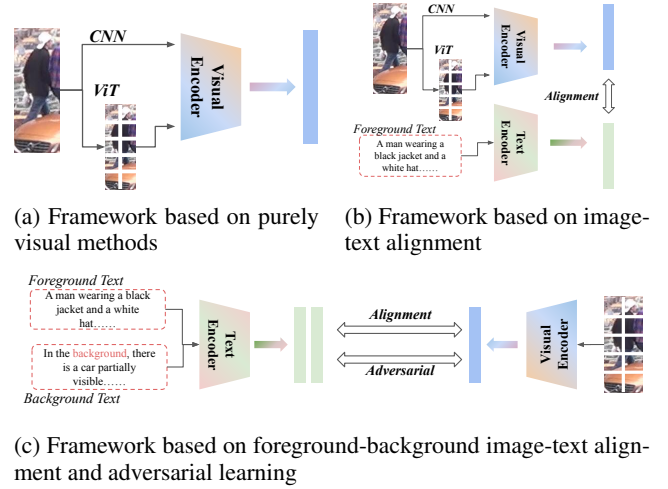


Figure 1: Frameworks of different person re-identification methods. (a) A framework purely based on vision model. (b) Include a vision model and a language model to align global or local image and text embeddings. (c) Our proposed framework, which is built upon intra-semantic alignment and inter-semantic adversarial learning.

local feature learning, employing strategies such as pose estimation (Wang et al. 2020), body segmentation (Huang et al. 2025; Kim et al. 2022), semantic segmentation (Gao et al. 2020; Zhu et al. 2020), and attention modules (Mao et al. 2023). However, these methods require auxiliary models and manual labels for preprocessing, and part-based segmentation techniques are not suitable for highly complex occlusion scenarios where the target’s body parts may be irregularly occluded. Meanwhile, data-driven methods aim to construct occlusion-enhanced data from existing datasets or manually generated samples (Tan et al. 2024; Xia et al. 2024; Wu et al. 2024). However, manually introducing occlusions cannot deal with complex or previously unseen scenarios, such as irregular objects like trees and handrails.

Some other methods explicitly differentiate foreground from background and apply a mask to indicate the target region (Liu et al. 2021; Yang et al. 2023; Liu et al. 2022). However, these methods do not genuinely understand the se-

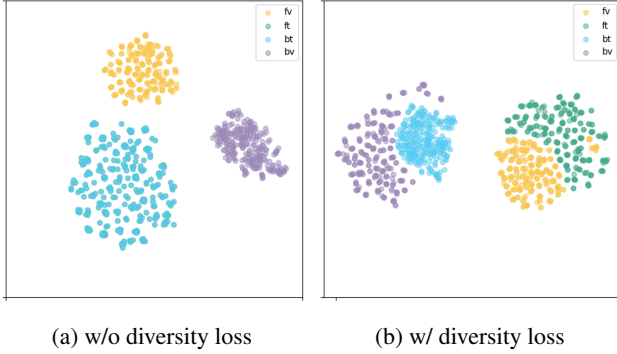


Figure 2: t-SNE visualization of cross-modal features, where each point represents an image feature. (a) Without diversity loss: ‘f’ and ‘b’ (foreground and background) features are entangled and ‘v’ and ‘t’ (visual and text) are misaligned. (b) With diversity loss: ‘v’ and ‘t’ features are well aligned, and ‘f’ and ‘b’ are clearly separated.

mantic content of images as humans do, and they are likely to miss the visual cues critical for identity recognition. *What do we, as human beings, think when we encounter someone we’ve met before?* The initial process involves filtering out background distractions while concurrently retrieving from memory visual cues of similar appearance, which aligns well with the challenges described above. CLIP-ReID (Li, Sun, and Li 2023), as the pioneer in aligning semantic and visual information in ReID, has achieved great performance in many benchmarks. Inspired by this success, more and more image-text based methods have been proposed to achieve better token-level and feature-level alignment (Yan et al. 2023; Jiang and Ye 2023; Wang et al. 2023; Yang and Zhang 2024; Wu et al. 2024). However, existing methods focus solely on modeling the foreground region and neglect the potentially informative background context. We argue that incorporating background information helps the model better distinguish semantic cues between foreground and background, reducing feature confusion when constraints or alignments are applied solely to the target region. Additionally, providing a semantic logit for the background enables the model to handle unseen or irregular background objects and textures that a purely visual pipeline would overlook.

In this paper, we propose FBA (Foreground and Background Adversarial Person Re-identification), a language-enhanced end-to-end framework that emulates human perception by jointly modeling foreground and background information in a cross-modal feature-extraction pipeline. To capture precise semantic cues of different components in the image and guide attention toward the target regions, the proposed framework is built upon **intra-semantic alignment** and **inter-semantic adversarial learning**, as shown in Fig. 1. The former adopts an alignment strategy similar to CLIP (Radford et al. 2021) to capture fine-grained multimodal features, while the latter introduces a diversity loss to help the model distinguish foreground targets from background distractions under the guidance of semantic information. Fig. 2 visualizes the

feature distances across different domains, providing insight into our strategy.

Unlike CLIP-based approaches that simply align global visual and text embeddings after encoding, we perform local patch-to-prompt intersections similar to (Yang et al. 2024) but employing a dual-branch cross-modal attention mechanism with four weight-shared cross-attention modules to associate image patches and prompt tokens belonging to the same semantic group. A shared four-layer self-attention module and feed-forward network further enhance both global and local fine-grained feature extraction. Following (Kang et al. 2025), who demonstrate that CLIP’s latent space lacks compositional expressivity, we retain all patch and token embeddings for local intersections. An attention map differential pooling strategy is then applied to filter out non-informative embeddings.

The main contributions of this work could be summarized as follows:

- We propose FBA, an end-to-end dual-branch cross-modal framework that treats both foreground and background semantics as equally important. It employs region-level visual-textual interaction to simulate human perception and capture fine-grained semantic cues.
- We introduce an intra-semantic alignment and inter-semantic adversarial learning strategy that aligns semantically consistent multimodal features and penalizes the feature distance between distractor and target regions.
- Our model achieves competitive results on both holistic and occluded ReID datasets, demonstrating its strong performance and generalization capability.

## Related Works

### Person Re-identification

Person re-identification has been studied for a long time, yet several critical challenges remain to be addressed. The primary challenges arise from diverse viewpoints, pose variations, noise interference, and occlusions. More generally, how to extract fine-grained features from the target region across multiple cameras while remaining robust to noise is still challenging. To capture local features, PCB (Sun et al. 2018) partitions the feature map into fixed horizontal stripes and learns independent part-level descriptors for each stripe. HOREID (Wang et al. 2020) utilizes high-order mapping of multilevel feature similarities to achieve fine-grained semantic pose alignment. ISP (Zhu et al. 2020) generates pseudo pixel-level labels for both body parts and personal belongings, then extracts local features of only the visible regions. PAT (Li et al. 2021) employs a transformer encoder-decoder to discover diverse part prototypes via pixel-context encoding and prototype-based decoding for robust occluded person ReID. TransReID (He et al. 2021), the first pure ViT-based ReID approach, extracts both global and local features with a jigsaw patch module and employs side-information embeddings to mitigate camera/view bias. With the powerful global receptive field, an increasing number of ViT-based methods have been proposed (Zhu et al. 2022; Tan et al. 2022; Zhu et al. 2023; Xia et al. 2024).

While these methods depend on improved feature alignment, other studies have adopted data-driven strategies, such as random erasing (Zhong et al. 2020) and manually generated samples (Wang et al. 2022a,b; Tan et al. 2024; Xia et al. 2024; Wu et al. 2024).

Other approaches explicitly distinguish between foreground and background, employing a mask to delineate the target region. FA-Net (Liu et al. 2021) introduces an end-to-end branch that explicitly localizes pedestrian foregrounds and extracts foreground-focused features. F-BDMTrack (Yang et al. 2023) employs fore-background distribution-aware attention within a transformer architecture to robustly discriminate targets and suppress background. However, these approaches lack human-level semantic understanding of images and may overlook visual cues in background that are essential for identity recognition.

## Vision-Language Pre-training

Recent work shows that large-scale vision-language pre-training (VLP) provides Re-ID models with richer semantic priors than image-only pre-training. General-purpose VLP models such as CLIP (Radford et al. 2021) learn aligned image-text representations, enabling the injection of textual cues (for example, clothing color or carried objects) that are difficult to capture using only RGB images. The pioneering CLIP-ReID (Li, Sun, and Li 2023) adopts a two-stage strategy. In the first stage, it trains a set of learnable text tokens for each image, similar to prompt learning in CoOp (Zhou et al. 2022). In the second stage, it optimizes the visual encoder. Inspired by it, various works have been focused on VLP based text-to-image person retrieval tasks. CFine (Yan et al. 2023) utilizes CLIP’s rich multi-modal knowledge to mine fine-grained intra-modal and inter-modal discriminative clues. IRRRA (Jiang and Ye 2023) adds random masking to text tokens and employs a token classifier after the cross attention layers to mine fine-grained global representations. TP-PS (Wang et al. 2023) further explores the modality association by constraints of various integrity and prompts for attribute hints. MGCC (Wu et al. 2024) applies a token selection mechanism to filter out non informative tokens and then feeds the remaining tokens into a global and local contrastive consistency alignment module. However, these methods restrict cross modal alignment to foreground features at both global and local levels, overlooking background semantic cues and the interaction between foreground and background that humans naturally use in similar recognition tasks.

## Preliminary

### Overview of CLIP-based Methods

Before introducing our proposed framework, we briefly review the CLIP-based methods. The CLIP and CLIP based methods align the visual and textual embeddings (namely class [CLS] and end [EOS] tokens) after visual encoder  $\mathcal{V}(\cdot)$  and text encoder  $\mathcal{T}(\cdot)$  with contrastive loss as in (Radford et al. 2021). The image-to-text contrastive loss is calculated

as:

$$\mathcal{L}_{i2t}(i) = -\log \frac{\exp(s(\mathbf{v}_i, \mathbf{t}_i))}{\sum_{j=1}^B \exp(s(\mathbf{v}_i, \mathbf{t}_j))} \quad (1)$$

where  $(\mathbf{v}_i, \mathbf{t}_i)$  denote the visual and textual embeddings of the  $i$ -th matched pair,  $s(\cdot, \cdot)$  is the similarity function (e.g., cosine similarity), and  $B$  is the batch size. The text-to-image contrastive loss shares the similar form. Derivative methods based on CLIP further address its limitation in handling multiple images of the same identity, which should ideally share similar textual descriptions (Li, Sun, and Li 2023; Yang et al. 2024).

Currently, many approaches focus on improving modality alignment and exploring the representational potential of CLIP in both vision and language. However, these methods often overlook the intuitive strategy adopted by humans in similar tasks, which involves first distinguishing between foreground and background. Although some methods based on masks or attention mechanisms have considered this characteristic, they do not effectively exploit the rich semantic information contained in the image, especially the background semantics that are present but usually ignored.

## Methodology

To address the aforementioned gap, we propose FBA, an adversarial ReID method that fully leverages interactions between foreground and background visual-semantic information to mimic human perception. It also exploits the great potential of CLIP embeddings.

### Multimodal Representation Encoding

To effectively capture both visual and textual information, we design a dual-stream encoding framework. The visual encoder  $\mathcal{V}(\cdot)$  is trainable, whereas the text encoder  $\mathcal{T}(\cdot)$  remains frozen to supply stable language priors. The foreground and background textual descriptions are generated from a large language model (Liu et al. 2023) with the prompts:

**Foreground Prompt:** “Describe the appearance of persons in the image, focusing on their appearance, attire and accessories.”

**Background Prompt:** “Describe the background in the image with less than 50 words, focusing on any objects or elements that might obscure the view of the person.”

The foreground text describes the target identity and background text provides contextual information. Note that the prompts are just simply selected and still need further exploration. These embeddings are then forwarded into the cross-modal interaction module.

### Dual-Branch Cross-modal Attention Module

To disentangle foreground and background semantics, we employ two parallel transformer branches, each consisting of a cross-attention module and fore stacked self-attention modules. The outputs from encoders are separated into two groups  $\{V_f, T_f\}$  and  $\{V_b, T_b\}$ . The subscripts  $f$  and  $b$  denote the foreground and background, respectively.  $V_{i \in (f,b)} =$

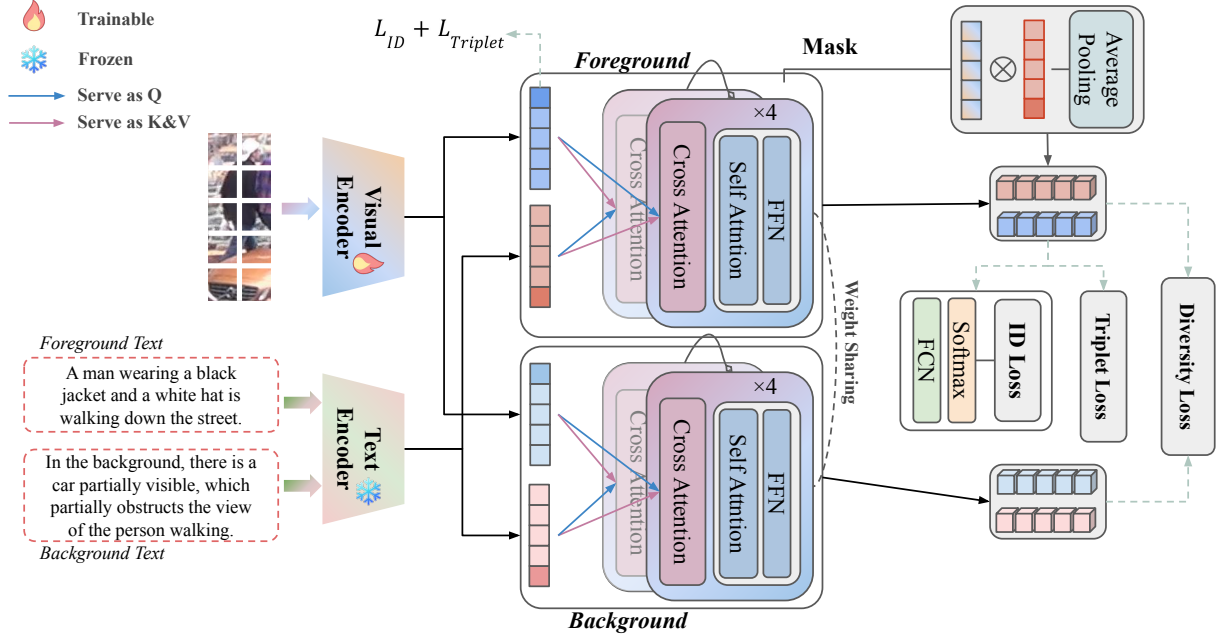


Figure 3: Overview of the proposed Foreground and Background Adversarial Image-text Person Re-identification framework (FBA). Embeddings from the visual and text encoders, including both foreground and background, are fed into a dual-branch cross-modal attention module. The model is optimized through intra-semantic alignment and inter-semantic adversarial learning to capture fine-grained semantic cues of different components and guide attention to target regions. Additionally, an attention map differential pooling strategy is applied to enhance informative patch selection.

$[[CLS], \mathbf{v}_i^1, \mathbf{v}_i^2, \dots, \mathbf{v}_i^N]$ , where  $N$  is the number of image patches.  $T_{i \in (f, b)} = [[SOS], \mathbf{t}_i^1, \mathbf{t}_i^2, \dots, \mathbf{t}_i^M, [EOS]]$ , where  $M$  is the number of text tokens. Most existing methods adopt image embeddings solely as *Key* and *Value* in cross-modal attention. In contrast, our method also utilizes image embeddings as *Query*, enabling a bidirectional interaction where both modalities can attend to each other more effectively. At the same time, all patches and tokens are preserved to fully exploit the fine-grained local cues. In summary, we adopt four weight shared Transformer blocks with two for foreground intersection and two for background.

The  $[CLS]$  and  $[EOS]$  tokens are then selected from the outputs of the attention module, specifically  $\{\mathcal{F}_f^T, \mathcal{F}_f^V\}$  for the foreground branch and  $\{\mathcal{F}_b^T, \mathcal{F}_b^V\}$  for the background branch. The superscripts  $V$  and  $T$  indicate that vision or text is used as the *Query*, respectively.

### Attention Map Differential Pooling

An attention map differential pooling strategy is proposed to further explore useful cues across all token embeddings, rather than focusing solely on the most critical ones. This idea is inspired by the work in (Kang et al. 2025). To apply more attention to tokens that better separate foreground and background, we first calculate the attention weights  $\mathcal{W}_f \in \mathbb{R}^{N \times M}$  from the cross-attention layer of the foreground branch and  $\mathcal{W}_b \in \mathbb{R}^{N \times M}$  from the background branch. To quantify the discrepancy between these two attention maps, we compute the cosine similarity between their correspond-

ing column vectors, resulting in an  $M$ -dimensional vector  $\mathbf{s} \in \mathbb{R}^{1 \times M}$ :

$$\mathbf{s}_j = \frac{\langle \mathcal{W}_f^{(:,j)}, \mathcal{W}_b^{(:,j)} \rangle}{\|\mathcal{W}_f^{(:,j)}\|_2 \cdot \|\mathcal{W}_b^{(:,j)}\|_2}, \quad j = 1, 2, \dots, M \quad (2)$$

We then apply a min-max normalization to this similarity vector to generate a token-wise attention mask  $\mathbf{m} \in \mathbb{R}^{1 \times M}$ :

$$\mathbf{m}_j = \frac{\mathbf{s}_j - \min(\mathbf{s})}{\max(\mathbf{s}) - \min(\mathbf{s})}, \quad j = 1, 2, \dots, M \quad (3)$$

This normalized mask is then used to aggregate the foreground text guided token embeddings as a pooling strategy. In other words, by focusing on tokens that exhibit stronger identity-related attention across foreground and background, the final feature representation incorporates richer identity cues.

### Objective Function

The overall framework is optimized using a combination of identity classification (ID) loss and triplet loss to ensure discriminative feature learning. These two losses are applied only to the foreground-guided features  $\mathcal{F}_f^T$  and  $\mathcal{F}_f^V$ , and the backbone foreground visual features.

$$\mathcal{L}_{ID} = -\frac{1}{B} \sum_{i=1}^B y_i \log \hat{y}_i \quad (4)$$

$$\mathcal{L}_{Triplet} = \max(\|f_a - f_p\|_2^2 - \|f_a - f_n\|_2^2 + m, 0) \quad (5)$$

In the ID loss,  $\hat{y}_i$  denotes the predicted probability of the ground-truth class  $y_i$ , and  $B$  is the batch size. In the triplet loss,  $f_a$ ,  $f_p$ , and  $f_n$  are the feature embeddings of the anchor, positive, and negative samples, respectively. The margin  $m$  controls the minimum distance between positive and negative pairs.

Additionally, to encourage feature diversity between foreground and background representations, we introduce a diversity loss that penalizes inter-semantic (fore-back) similarity while promoting intra-semantic (fore-fore and back-back) alignment.

$$\mathcal{L}_{\text{tri-div}} = \sum_{(a,b|c,d) \in \mathcal{P}} \mathcal{L}_{\text{Triplet}}^{a,b|c,d} \quad (6)$$

$$\mathcal{L}_{\text{con}} = (1 - s(\mathcal{F}_f^T, \mathcal{F}_f^V)) + (1 - s(\mathcal{F}_b^T, \mathcal{F}_b^V)) \quad (7)$$

$$\mathcal{L}_{\text{div}} = \mathcal{L}_{\text{tri-div}} + \mathcal{L}_{\text{con}} \quad (8)$$

where  $\mathcal{L}_{\text{Triplet}}^{a,b|c,d}$  denotes the triplet loss computed between one positive pair  $(a, b)$  and two negative pairs  $(a, c)$  and  $(a, d)$ . The set  $\mathcal{P}$  contains all four complementary configurations between foreground and background features, and all possible pairs will be calculated twice:

$$\mathcal{P} = \left\{ \begin{array}{l} (\mathcal{F}_f^T, \mathcal{F}_f^V | \mathcal{F}_b^T, \mathcal{F}_b^V), \\ (\mathcal{F}_b^T, \mathcal{F}_b^V | \mathcal{F}_f^T, \mathcal{F}_f^V), \\ (\mathcal{F}_f^V, \mathcal{F}_f^T | \mathcal{F}_b^T, \mathcal{F}_b^V), \\ (\mathcal{F}_b^V, \mathcal{F}_b^T | \mathcal{F}_f^T, \mathcal{F}_f^V), \end{array} \right\} \quad (9)$$

While  $\mathcal{L}_{\text{tri-div}}$  provides a multi-view triplet-based alignment between foreground and background features across modalities, it focuses primarily on the relative distance between positive and negative samples. To further enhance the absolute consistency of modality-specific representations, we introduce an auxiliary contrastive loss  $\mathcal{L}_{\text{con}}$ , which directly encourages similarity between paired text and visual features within the same semantic region.

The overall objective function combines identity loss, triplet loss, and proposed diversity loss. The training objective is formulated as follows:

$$\mathcal{L}_{\text{total}} = \mathcal{L}_{\text{ID}} + \mathcal{L}_{\text{Triplet}} + \mathcal{L}_{\text{ID}}^C + \mathcal{L}_{\text{Triplet}}^C + \lambda \mathcal{L}_{\text{div}} \quad (10)$$

where the superscript  $C$  denotes the loss generated from cross-modal features. The hyperparameter  $\lambda$  balances the contribution of the diversity loss.

## Experiments

### Experimental Setting

**Datasets and Evaluation Protocols.** The proposed method in this work is fully evaluated through four person re-identification datasets, including two holistic datasets DukeMTMC-reID (Zheng, Zheng, and Yang 2017) and CUHK03-NP (labeled) (Li et al. 2014), and two occluded datasets Occluded-Duke (Miao et al. 2019) and Occluded-ReID (Zhuo et al. 2018). The details of those datasets are summarized in Table 2. Following established practices, we adopt mean Average Precision (mAP) and Rank-1 (R-1) accuracy as the primary evaluation metrics.

**Implementation Details.** We adopt the ViT-B/16 model pre-trained by CLIP as our backbone with a sliding-window setting as in (He et al. 2021). The visual backbone consists of 12 transformer layers with a hidden size of 768. A linear projection layer is used to map the 512-dimensional output of the text encoder to 768 dimensions. Foreground and background captions are generated using the LLaVA v1.5-7b model (Liu et al. 2023). All input images are resized to  $384 \times 128$ , with a batch size of 64, comprising 16 identities and 4 images per identity. We use the Adam optimizer with a weight decay of  $1e-4$ . The model is trained for 60 epochs, including 10 warm-up epochs during which the learning rate increases linearly from  $0.001 \times \text{base learning rate}$  to the base learning rate, followed by a cosine decay to  $0.01 \times \text{base learning rate}$ . To accommodate the varying scale and complexity of different datasets, we empirically set the base learning rate for each dataset:  $8e-5$  for DukeMTMC-reID and Occluded-Duke, and  $1.2e-4$  for CUHK03-NP. Note that the Occluded-ReID is used only as a test set. This per-dataset adjustment improves training stability and convergence performance. The margin  $m$  for the triplet loss is set to 0.3, and the balance factor in Eq. (10) is  $\lambda = 0.5$ . The entire framework is implemented using PyTorch and trained on 4 NVIDIA A6000 GPUs.

### Comparison with State-of-the-art Methods

This section compares our proposed method with several state-of-the-art approaches, including those based on CNN and ViT backbones. A detailed analysis of the results presented in Table 1 is provided below.

**Holistic ReID.** We compare the performance of FBA with several existing methods on two holistic person ReID datasets. On DukeMTMC, FBA achieves a notable improvement over the baseline (+1.7% mAP, +2.7% R-1), and surpasses previous state-of-the-art methods in terms of R-1 accuracy, although its mAP does not exceed all methods listed in the table. This result suggests that the integration of foreground-background semantic information with visual features enhances the model’s ability to handle more challenging samples (as reflected in R-1). However, the overall effect of the adversarial learning appears limited. We speculate this may be due to the complex and irregular nature of background noise in DukeMTMC, where multiple individuals often appear in the same image, leading to less precise background descriptions.

On the CUHK03-NP benchmark, our approach surpasses all existing methods, achieving 2.2% mAP and 1.5% R-1 improvement over PromptSG (Yang et al. 2024). This demonstrates that the introduction of multimodal interaction and the diversity loss effectively enhances the model’s ability to distinguish between foreground and background content.

**Occluded ReID.** Although our method does not incorporate explicit mechanisms designed for occlusion handling, as seen in works such as HOREID (Wang et al. 2020), ISP (Zhu et al. 2020), PAT (Li et al. 2021), FA-Net (Liu et al. 2021), FED (Wang et al. 2022b), and AAFormer (Zhu et al. 2023), we still evaluate it on two occluded ReID datasets. This is because the adversarial learning design in our method is intrinsically capable of suppressing interference from obstruc-



Table 1: Comparison of CNN- and ViT-based methods on DukeMTMC, CUHK03-NP (labeled), Occluded-Duke, and Occluded-ReID datasets.

Backbone	Method	Reference	DukeMTMC		CUHK03-NP		Occluded-Duke		Occluded-ReID	
			mAP	R-1	mAP	R-1	mAP	R-1	mAP	R-1
CNN	PCB	ECCV'2018	69.2	83.3	57.5	63.7	-	-	-	-
	DSR	CVPR'2018	-	-	-	-	30.4	40.8	62.8	72.8
	OSNet	ICCV'2019	73.5	88.6	67.8	72.3	-	-	-	-
	HOReID	CVPR'2020	75.6	86.9	-	-	43.8	55.1	70.2	80.3
	PVPM	CVPR'2020	-	-	-	-	37.7	47.0	59.5	66.8
	ISP	ECCV'2020	80.0	89.6	74.1	76.5	52.3	62.8	-	-
	PAT	CVPR'2021	78.2	88.8	-	-	53.6	64.5	72.1	81.6
	FA-Net	TIP'2021	77.0	88.7	-	-	-	-	-	-
	Part-Label	ICCV'2021	-	-	-	-	46.3	62.2	71.0	81.0
	LTReID	TMM'2022	80.4	90.5	80.3	82.1	-	-	-	-
	DRL-Net	TMM'2022	76.6	88.1	-	-	50.8	65.0	-	-
	CLIP-ReID	AAAI'2023	80.7	90.0	-	-	53.5	61.0	-	-
	PromptSG	CVPR'2024	80.4	90.2	79.8	80.5	-	-	-	-
ViT	TransReID	ICCV'2021	82.0	90.7	-	-	59.2	66.4	-	-
	DCAL	CVPR'2022	80.1	89.0	-	-	-	-	-	-
	FED	CVPR'2022	78.0	89.4	-	-	56.4	68.1	79.3	86.3
	AAFormer	TNNLS'2023	80.9	90.1	79.0	80.3	58.2	67.1	-	-
	CLIP-ReID	AAAI'2023	82.5	90.0	-	-	59.5	67.1	-	-
	PromptSG	CVPR'2024	81.6	91.0	83.1	85.1	-	-	-	-
	Baseline		80.0	88.8	82.9	84.8	53.5	60.8	74.0	76.3
	FBA	Ours	81.7	91.5	85.3	86.6	60.5	69.5	84.0	85.4

Table 2: Statistics of ReID datasets in our experiments.

Dataset	IDs	Images	Cams
DukeMTMC-reID	1,404	36,411	8
CHUK03-NP	1,467	13,164	2
Occluded-Duke	1,404	35,489	8
Occluded-ReID	200	2,000	-

tions.

On Occluded-Duke, FBA outperforms all other methods (+1.0% mAP, +1.4% R-1). For Occluded-ReID, which is a test-only dataset, we use the model trained on CUHK03-NP and obtain 84% mAP, surpassing previous records, with Rank-1 accuracy second only to FED. These results highlight the generalization capability of FBA.

## Ablation Studies

**Contributions from Different Components.** To quantitatively analyze the contribution of each component in our approach, we conduct ablation studies on the DukeMTMC and CUHK03-NP datasets, as shown in Table 3.

In the first row, the baseline model uses the features extracted by the backbone visual encoder to compute the losses ( $\mathcal{L}_{ID} + \mathcal{L}_{Triplet}$ ). In the second row, the cross-modal interaction module is introduced, but only the foreground textual information is involved in the cross-attention. Comparing

the first and second rows, the introduction of cross-modal interaction leads to a noticeable improvement in Rank-1 accuracy. The third row introduces the diversity loss, bringing improvements in both mAP and Rank-1 accuracy. In the last row, we incorporate the attention map differential pooling strategy, which allows the model to aggregate information beyond a single token for global representation. On the DukeMTMC dataset, this module leads to significant gains in both mAP and Rank-1 accuracy, and also brings moderate improvements on CUHK03-NP. At this stage, all components together constitute the complete FBA architecture.

**Ablation Study on Image Size and Stride Size.** We compare the performance of FBA on the CUHK03-NP dataset under different image sizes and stride settings, as shown in Table 4. When increasing the image resolution from  $256 \times 128$  to  $384 \times 128$ , the Rank-1 accuracy remains nearly unchanged, while the mAP improves by 0.5%. A reduction in stride size from 16 to 12 notably improves performance, yielding a 1.3% increase in mAP and a 1.3-1.4% rise in Rank-1 accuracy. This suggests that a smaller stride enables the model to capture more fine-grained features. Notably, even under the least optimal configuration, our method still outperforms other approaches.

## Qualitative Analysis

To better demonstrate the effectiveness of our method in distinguishing foreground from background, we visualize the attention maps, as shown in Fig. 4. The first row presents

Table 3: Ablation study on the effectiveness of each loss component on DukeMTMC and CUHK03-NP.

Components				DukeMTMC				CUHK03-NP			
$\mathcal{L}_{ID} + \mathcal{L}_{Triplet}$	$\mathcal{L}_{ID}^C + \mathcal{L}_{Triplet}^C$	$\mathcal{L}_{div}$	$Mask$	mAP	R-1	R-5	R-10	mAP	R-1	R-5	R-10
✓				80.0	88.0	94.5	95.9	82.9	84.8	93.2	96.4
✓	✓			80.0	90.3	94.6	95.6	83.1	85.0	93.1	96.8
✓	✓	✓		80.7	90.4	94.6	96.1	84.9	86.3	94.1	97.1
✓	✓	✓	✓	<b>81.7</b>	<b>91.5</b>	<b>95.3</b>	<b>96.3</b>	<b>85.3</b>	<b>86.6</b>	<b>94.3</b>	<b>97.1</b>

Table 4: Ablation analysis of different image and stride sizes during training on CUHK03-NP.

Image Size	Stride Size	mAP	R-1
256×128	16	83.5	85.3
384×128	16	84.0	85.2
256×128	12	84.8	86.6
384×128	12	85.3	86.6

the original images, while the second row displays the corresponding images overlaid with attention heatmaps. We directly extract the attention weights from the cross-attention layer.

The figure illustrates attention maps from samples in the Occluded-Duke and Occluded-ReID datasets, which include various types of occlusions such as vehicles, railings, and non-target pedestrians, presenting considerable challenges. Our method demonstrates a strong ability to understand the semantic structure of foreground and background regions and to distinguish target person from distracting elements.

For instance, in the first column of Occluded-Duke, FBA effectively identifies and suppresses interference from vehicles in the scene, directing attention to key attributes of the target individual such as the coat, backpack, and hair. In the second column, despite the presence of a distracting pedestrian with a backpack in front of the target, our method accurately avoids the interference. In the third column of Occluded-ReID, the target person is occluded by multiple layers of metal railings. Remarkably, the model focuses precisely on the person, avoiding the railings, and is even able to capture the body parts visible between the bars.

## Conclusion

This paper proposes a language-enhanced end-to-end foreground-background adversarial framework for person re-identification, named FBA. By employing a dual-branch cross-modal attention mechanism, FBA simultaneously models foreground and background semantics. A diversity loss and an attention map-based differential pooling strategy are further introduced to effectively distinguish target regions from background distractions, enhancing the model’s discriminative ability in complex scenes. Experimental results show that FBA achieves or approaches state-of-the-art performance in terms of mAP and Rank-1 accuracy on four benchmark datasets: DukeMTMC-reID, CUHK03-NP,

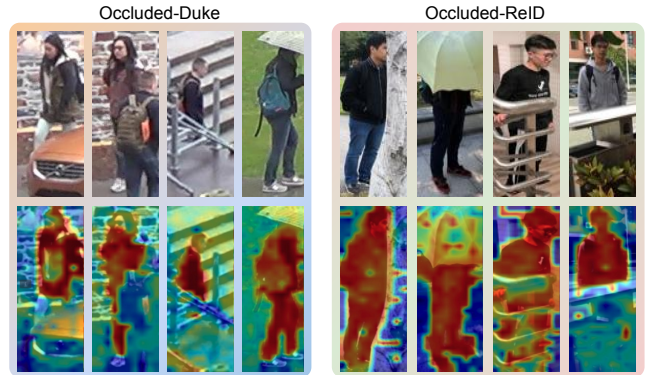


Figure 4: Attention map visualization of FBA on Occluded-Duke and Occluded-ReID. The first row represents the raw images and the second row presents the attention maps.

Occluded-Duke, and Occluded-ReID. This validates its generalization and robustness in both holistic and occluded person re-identification tasks.

Nevertheless, there is still room for improvement. In future work we plan to explore more refined prompt engineering and more efficient, lightweight model designs to further enhance feasibility for large-scale and real-time deployment.

## References

- Gao, L.; Zhang, H.; Gao, Z.; Guan, W.; Cheng, Z.; and Wang, M. 2020. Texture semantically aligned with visibility-aware for partial person re-identification. In *Proceedings of the 28th ACM international conference on multimedia*, 3771–3779.
- He, S.; Luo, H.; Wang, P.; Wang, F.; Li, H.; and Jiang, W. 2021. Transreid: Transformer-based object re-identification. In *Proceedings of the IEEE/CVF international conference on computer vision*, 15013–15022.
- Huang, K.; Azfar, T.; Reilly, J.; and Ke, R. 2025. TransitReID: Transit OD Data Collection with Occlusion-Resistant Dynamic Passenger Re-Identification. *arXiv preprint arXiv:2504.11500*.
- Jiang, D.; and Ye, M. 2023. Cross-modal implicit relation reasoning and aligning for text-to-image person retrieval. In *Proceedings of the IEEE/CVF Conference on Computer Vision and Pattern Recognition*, 2787–2797.
- Kang, R.; Song, Y.; Gkioxari, G.; and Perona, P. 2025.

Is CLIP ideal? No. Can we fix it? Yes! *arXiv preprint arXiv:2503.08723*.

Kim, M.; Cho, M.; Lee, H.; Cho, S.; and Lee, S. 2022. Occluded person re-identification via relational adaptive feature correction learning. In *ICASSP 2022-2022 IEEE International Conference on Acoustics, Speech and Signal Processing (ICASSP)*, 2719–2723. IEEE.

Li, S.; Sun, L.; and Li, Q. 2023. Clip-reid: exploiting vision-language model for image re-identification without concrete text labels. In *Proceedings of the AAAI conference on artificial intelligence*, volume 37, 1405–1413.

Li, W.; Zhao, R.; Xiao, T.; and Wang, X. 2014. Deep-reid: Deep filter pairing neural network for person re-identification. In *Proceedings of the IEEE conference on computer vision and pattern recognition*, 152–159.

Li, Y.; He, J.; Zhang, T.; Liu, X.; Zhang, Y.; and Wu, F. 2021. Diverse part discovery: Occluded person re-identification with part-aware transformer. In *Proceedings of the IEEE/CVF conference on computer vision and pattern recognition*, 2898–2907.

Liu, D.; Han, S.; Chen, Y.; Xia, C.; and Zhao, J. 2022. Foreground-guided textural-focused person re-identification. *Neurocomputing*, 483: 235–248.

Liu, H.; Li, C.; Wu, Q.; and Lee, Y. J. 2023. Visual Instruction Tuning.

Liu, Y.; Zhou, W.; Liu, J.; Qi, G.-J.; Tian, Q.; and Li, H. 2021. An end-to-end foreground-aware network for person re-identification. *IEEE Transactions on Image Processing*, 30: 2060–2071.

Mao, J.; Yao, Y.; Sun, Z.; Huang, X.; Shen, F.; and Shen, H.-T. 2023. Attention map guided transformer pruning for occluded person re-identification on edge device. *IEEE Transactions on Multimedia*, 25: 1592–1599.

Miao, J.; Wu, Y.; Liu, P.; Ding, Y.; and Yang, Y. 2019. Pose-guided feature alignment for occluded person re-identification. In *Proceedings of the IEEE/CVF international conference on computer vision*, 542–551.

Ning, E.; Wang, C.; Zhang, H.; Ning, X.; and Tiwari, P. 2024. Occluded person re-identification with deep learning: a survey and perspectives. *Expert systems with applications*, 239: 122419.

Radford, A.; Kim, J. W.; Hallacy, C.; Ramesh, A.; Goh, G.; Agarwal, S.; Sastry, G.; Askell, A.; Mishkin, P.; Clark, J.; et al. 2021. Learning transferable visual models from natural language supervision. In *International conference on machine learning*, 8748–8763. PmlR.

Sun, Y.; Zheng, L.; Yang, Y.; Tian, Q.; and Wang, S. 2018. Beyond part models: Person retrieval with refined part pooling (and a strong convolutional baseline). In *Proceedings of the European conference on computer vision (ECCV)*, 480–496.

Tan, L.; Dai, P.; Ji, R.; and Wu, Y. 2022. Dynamic prototype mask for occluded person re-identification. In *Proceedings of the 30th ACM international conference on multimedia*, 531–540.

Tan, L.; Xia, J.; Liu, W.; Dai, P.; Wu, Y.; and Cao, L. 2024. Occluded person re-identification via saliency-guided patch transfer. In *Proceedings of the AAAI conference on artificial intelligence*, volume 38, 5070–5078.

Wang, G.; Yang, S.; Liu, H.; Wang, Z.; Yang, Y.; Wang, S.; Yu, G.; Zhou, E.; and Sun, J. 2020. High-order information matters: Learning relation and topology for occluded person re-identification. In *Proceedings of the IEEE/CVF conference on computer vision and pattern recognition*, 6449–6458.

Wang, G.; Yu, F.; Li, J.; Jia, Q.; and Ding, S. 2023. Exploiting the textual potential from vision-language pre-training for text-based person search. *arXiv preprint arXiv:2303.04497*.

Wang, P.; Zhao, Z.; Su, F.; and Meng, H. 2022a. Lt-reid: Factorizable feature generation with independent components for long-tailed person re-identification. *IEEE Transactions on Multimedia*, 25: 4610–4622.

Wang, Z.; Zhu, F.; Tang, S.; Zhao, R.; He, L.; and Song, J. 2022b. Feature erasing and diffusion network for occluded person re-identification. In *Proceedings of the IEEE/CVF conference on computer vision and pattern recognition*, 4754–4763.

Wu, X.; Ma, W.; Guo, D.; Zhou, T.; Zhao, S.; and Cai, Z. 2024. Text-based occluded person re-identification via multi-granularity contrastive consistency learning. In *Proceedings of the AAAI conference on artificial intelligence*, volume 38, 6162–6170.

Xia, J.; Tan, L.; Dai, P.; Zhao, M.; Wu, Y.; and Cao, L. 2024. Attention disturbance and dual-path constraint network for occluded person re-identification. In *Proceedings of the AAAI Conference on Artificial Intelligence*, volume 38, 6198–6206.

Yan, S.; Dong, N.; Zhang, L.; and Tang, J. 2023. Clip-driven fine-grained text-image person re-identification. *IEEE Transactions on Image Processing*, 32: 6032–6046.

Yang, D.; He, J.; Ma, Y.; Yu, Q.; and Zhang, T. 2023. Foreground-background distribution modeling transformer for visual object tracking. In *Proceedings of the IEEE/CVF international conference on computer vision*, 10117–10127.

Yang, S.; and Zhang, Y. 2024. MLLMReID: multimodal large language model-based person re-identification. *arXiv preprint arXiv:2401.13201*.

Yang, Z.; Wu, D.; Wu, C.; Lin, Z.; Gu, J.; and Wang, W. 2024. A pedestrian is worth one prompt: Towards language guidance person re-identification. In *Proceedings of the IEEE/CVF Conference on Computer Vision and Pattern Recognition*, 17343–17353.

Zheng, Z.; Zheng, L.; and Yang, Y. 2017. Unlabeled samples generated by gan improve the person re-identification baseline in vitro. In *Proceedings of the IEEE international conference on computer vision*, 3754–3762.

Zhong, Z.; Zheng, L.; Kang, G.; Li, S.; and Yang, Y. 2020. Random erasing data augmentation. In *Proceedings of the AAAI conference on artificial intelligence*, volume 34, 13001–13008.



- Zhou, K.; Yang, J.; Loy, C. C.; and Liu, Z. 2022. Learning to prompt for vision-language models. *International Journal of Computer Vision*, 130(9): 2337–2348.
- Zhu, H.; Ke, W.; Li, D.; Liu, J.; Tian, L.; and Shan, Y. 2022. Dual cross-attention learning for fine-grained visual categorization and object re-identification. In *Proceedings of the IEEE/CVF conference on computer vision and pattern recognition*, 4692–4702.
- Zhu, K.; Guo, H.; Liu, Z.; Tang, M.; and Wang, J. 2020. Identity-guided human semantic parsing for person re-identification. In *Computer Vision–ECCV 2020: 16th European Conference, Glasgow, UK, August 23–28, 2020, Proceedings, Part III 16*, 346–363. Springer.
- Zhu, K.; Guo, H.; Zhang, S.; Wang, Y.; Liu, J.; Wang, J.; and Tang, M. 2023. Aaformer: Auto-aligned transformer for person re-identification. *IEEE Transactions on Neural Networks and Learning Systems*.
- Zhuo, J.; Chen, Z.; Lai, J.; and Wang, G. 2018. Occluded person re-identification. In *2018 IEEE international conference on multimedia and expo (ICME)*, 1–6. IEEE.